Enhanced stimulated Raman scattering by femtosecond ultraviolet plasma grating in water

Fengjiang Liu, Shuai Yuan, Boqu He, Junyi Nan, Abdul Qayyum Khan, Liang'en Ding, and Heping Zeng

Citation: Appl. Phys. Lett. **112**, 094101 (2018); doi: 10.1063/1.5018629
View online: https://doi.org/10.1063/1.5018629
View Table of Contents: http://aip.scitation.org/toc/apl/112/9
Published by the American Institute of Physics

Enhanced stimulated Raman scattering by femtosecond ultraviolet plasma grating in water

Fengjiang Liu,[1] Shuai Yuan,[2] Boqu He,[1] Junyi Nan,[1] Abdul Qayyum Khan,[1] Liang'en Ding,[1] and Heping Zeng[1,2,a)]
[1]*State Key Laboratory of Precision Spectroscopy, East China Normal University, Shanghai 200062, China*
[2]*Shanghai Key Laboratory of Modern Optical System, Engineering Research Center of Optical Instrument and System (Ministry of Education), School of Optical-Electrical and Computer Engineering, University of Shanghai for Science and Technology, Shanghai 200093, China*

(Received 8 December 2017; accepted 16 February 2018; published online 28 February 2018)

Efficient forward stimulated Raman scattering (SRS) was observed along 400-nm femtosecond (fs) laser filaments in water. SRS conversion dominated over self-phase modulation induced continuum generation as the input pulse energy was above 4 μJ ($\sim$30 P_{cr}), implying that plasma in the aqueous filamentation channel played an important role in compensating for the group velocity walk-off between the pump and Stokes pulses. By overlapping two synchronous fs 400-nm filaments to form plasma grating in water, significant enhancement of SRS conversion was observed. Such a SRS enhancement originated from the ultrahigh plasma density in the intersection region of the preformed plasma grating. *Published by AIP Publishing.* https://doi.org/10.1063/1.5018629

Femtosecond (fs) laser filamentation is a well-known optical nonlinear process that has raised much interest in the last decade for potential applications ranging from remote sensing,[1] lightning protection[2] to, more recently, frequency conversion.[3–5] When laser peak power exceeds a critical value, filamentation appears spontaneously due to the dynamic balance between Kerr self-focusing and plasma defocusing of the medium, and the laser intensity remains stable in the core of the beam over an extended propagation distance.[6] In condensed media with normal group velocity dispersion (GVD), laser filamentation is interpreted in terms of the dynamical interaction of spontaneously generated X waves, which are a particular class of conical waves with the notable feature of being stationary, i.e., nondispersive and nondiffractive.[5–9] Specifically, stimulated Raman scattering (SRS) that transfers part of laser energy to a red-shifted wavelength during laser filamentation has been shown to possess very high conversion efficiency in some liquids, which is due to the spontaneous formation of nonlinear X waves at the Stokes Raman wavelength, and more importantly, the group velocity matching (GVM) between the pump and Raman X pulses.[5] Motivated by applications including potential Raman lasers, advanced laser acoustic generation, laser ophthalmological surgery, and chemical reaction probing, nonlinear processes during laser filamentation in water are of special interest, and many experimental studies on the SRS process in water have been reported.[10–14] However, most of the previous work utilized picosecond or nanosecond green lasers at wavelength around 532 nm as pumping sources, mainly due to the easy availability of these laser sources.[11,14] While with fs lasers at ultraviolet exciting wavelength, which is close to the minimum of water absorption, the investigation on SRS processes during laser filamentation in water remains blank.

As the most common and important liquid on earth, water essentially has a not-very-high Raman gain as compared to common organic liquids (e.g., ethanol). The dominant Raman peak of liquid water around 3450 cm^{-1} originates from the OH bond stretching vibration.[15,16] It is different from nonlinear processes such as harmonic generation and four-wave mixing, where phase matching of wave vectors plays an important role; efficient Raman conversion relies heavily on the GVM of the pump pulse and the Raman pulse, as it is intrinsically phase-matched during the conversion process with the vibratory medium being an intermediary.[5] Recently, laser plasma grating induced by interference of two noncollinear fs filaments was demonstrated to generate ultrahigh local electron density in their intersection region in water, which was due to the much higher optical intensity at the positive interference fringes, and the local electron density was beyond its typical value limited by an intensity-clamped filament.[17] Previous work suggested that plasma grating in air gave rise to interesting physics including laser energy exchange,[18–20] diffraction of a third beam,[21,22] and enhanced third harmonic generation,[23] which originated from the interaction of two filaments and the spatially modulated ultrahigh electron density along interference fringes in the intersection region. Inspired by those experiments, it is also intriguing to explore the impact of plasma grating on water Raman conversion.

In this paper, we report experimental observation on intense forward SRS in water with fs UV filamentation at 400 nm. At this wavelength, we showed that when laser peak power was sufficiently high, Raman conversion dominated the spectral change during laser filamentation rather than self-phase modulation (SPM) induced continuum, implying that plasma in the aqueous filamentation channel played an important role in compensating for the group velocity walk-off between the pump and Stokes pulses. Moreover, by overlapping two UV filaments with a small crossing angle to form plasma grating in water, significantly enhanced SRS emission at 463 nm was observed. We attributed this phenomenon to the compensation of GVD due to the ultrahigh local electron density of plasma grating, which acted as a

a)Author to whom correspondence should be addressed: hpzeng@phy.ecnu.edu.cn

buffer area for pulse self-compression. The enhanced SRS emission mechanism revealed in this paper may be of directive significance for applications in intense Raman lasers and fs Raman spectroscopy.

Intense 400-nm fs pulses with a pulse energy up to 3 mJ and a full width at half maximum (FWHM) diameter of 6 mm were generated by passing 800 nm fundamental-wave pulses of a Ti:sapphire regenerative laser (130 fs, 15 mJ, 10 Hz) through a β-barium borate (β-BBO) crystal of 0.2 mm thickness. The fundamental-wave laser and the thin crystal were adjusted to their best conditions as to achieve the highest frequency-doubling efficiency, so the pulse duration of the 400-nm pulses was believed to be roughly the same as the fundamental-wave pulses. After passing through a tunable attenuator (fused silica) of 2 mm thickness for energy adjusting, the generated 400-nm pulses were split into pump and probe beams by means of a UV beam splitter with an energy ratio of about 2:3. With one beam applied by a delay line for pulse synchronization adjustment, the two beams were finally transferred in parallel to a planoconvex focal lens (f = 150 mm) to generate two noncollinear filaments, which overlapped each other with a crossing angle of ~4° at the focus of the lens. The polarizations of two beams were orthogonal to their intersection plane. A fused silica cuvette with 50 mm length was placed after the lens. The fore and rear walls of the cuvette were both 2 mm thick. The crossing point of two filaments was located in the middle of the cuvette when the cuvette was filled with water. To visualize the filaments and assist synchronization adjustment in water, 1 μl of commercially available aqueous colloidal gold (NS-60–50, NanoSeedz) was doped into 25 ml distilled water in the cuvette as scattering media as implemented in Ref. 17. Figure 1 schematically shows the formation of plasma grating as two beams temporally overlap each other in water. In their intersection region, interference of two beams resulted in periodic optical fields, as shown in the inset of Fig. 1, which was taken by a CCD camera equipped on a 10× microscope (see Ref. 17 for details). The full width and the length of the plasma grating were about 70 μm and 2 mm, respectively. Once the periodic scattering fringes showed their best fringe contrast, rigid synchronization (zero time delay) of two beams was confirmed, and in the following experiments, the liquid was replaced by pure water, as is the

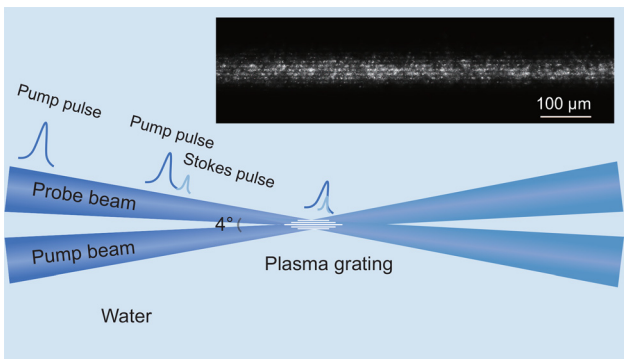

FIG. 1. Schematic of plasma grating formation in water. The inset shows the interference fringes of plasma grating when two beams were synchronized (zero time delay) in dilute aqueous colloidal gold with the total input pulse energy of 25 μJ.

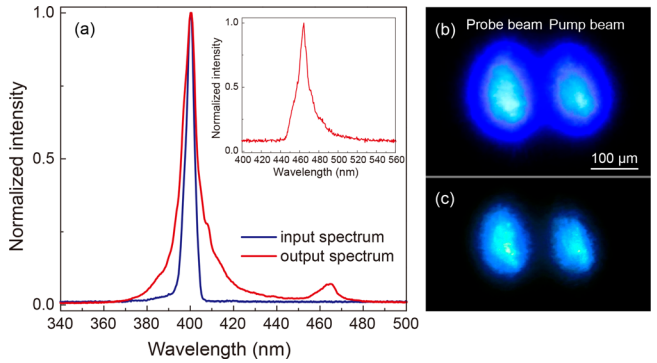

FIG. 2. Forward SRS emission during 400-nm fs filamentation in water. (a) Spectra of the probe beam before and after it underwent filamentation in water. The inset spectrum shows the clean Raman peak after passing the 450 nm long-pass filter. (b) and (c) are the light spots of two asynchronous beams after propagation in water and projected onto a white paper after collimation without (b) and with (c) the 450 nm long-pass filter, respectively. The pulse energy of the probe beam and the pump beam was 10 μJ and 7 μJ, respectively.

research object in this study. Here, we used the extended concept of plasma grating, namely, as long as two coherent pulses had an overlap in time domain, the interference of their filaments was called plasma grating, even if the overlap was partial or the interference fringes deteriorated. After the cuvette, a fused silica planoconvex lens with a focal length of 50 mm was used to collimate the output conical emission of the two beams, and the light spots of the two beams were spatially separated in the output [see Fig. 2(b)]. To study the Raman properties of single beam filamentation in water and the effect of plasma grating on the Raman conversion in water, a beam dump was used to block the pump beam before and after the cuvette, respectively. A long-pass filter with a cut-on wavelength of 450 nm (FEL0450) was used to filter out the 400 nm pump signal when measuring the energy of the Raman signal in the output probe beam. As the spectra of the conical Raman signal were spatially dispersive,[5] the output of the probe beam after collimation was converged to a small point using lenses, and the spectra were measured using a fiber spectrometer (Maya2000 Pro, Ocean Optics) with a neutral density filter (OD: 1.0) for attenuation. All experiments were performed at ambient temperature and pressure.

The critical power ($P_{cr} = 3.77\lambda^2/8\pi n_0 n_2$) for laser filamentation in water is ~1 MW for 400 nm laser,[6] which is about three orders lower than that of air. Femtosecond pulse energy as low as hundreds of nanojoules at this wavelength is able to create a filament in water and then modify the spectrum.[24] Figure 2 shows the spectral and beam evolution as the laser undergoes filamentation in water. The pulse energy of the probe beam was set as 10 μJ, corresponding to ~73 P_{cr}. Intense SRS emission at ~463 nm was observed in the forward direction, as spectrally shown in Fig. 2(a). The Raman peak was distinct in the weak continuum background and possessed a FWHM linewidth of 12 nm (560 cm^{-1}). Note that it was much broader than the normal SRS linewidth of water (e.g., ~200 cm^{-1} in Ref. 5), which was generally considered to arise from self-focusing of the Raman pulse,[13,16] and the other way round it indicated the high intensity of the Raman pulse. Unlike infrared filaments that

can generate supercontinuum covering the whole visible region in water,[6] spectral broadening by UV filaments is quite limited, which is similar to that in air and is attributable to the much lower clamped intensity of UV filaments.[25,26] When two beams were far away from synchronization and both entered the cuvette, their output light spots projected onto a white paper after collimation without and with the 450 nm long-pass filter as shown in Figs. 2(b) and 2(c), respectively. After the filter, the output pulses could be regarded as pure Stokes Raman pulses [see the inset spectrum in Fig. 2(a)]. The Raman pulses had a slightly smaller conical angle than the pump pulses after propagation in water and they shared the same central optical axes, as well as good directivity, which implied that it came from a stimulated process. It was quite different from the experimental results of Jarnac *et al.* that no apparent Raman effect emerged as a similar 400-nm, 100-fs pulse underwent filamentation in water.[24] In their experiments, laser peak power was varied from 0.6 to 9 P_{cr} and the output spectra took on conventional broadening which extended mainly into the red due to SPM. However, we showed that when the peak power of the laser pulse was sufficiently high, Raman conversion became noteworthy and an impressive part of laser energy was transferred to the Raman peak. As we will see below, the pulse energy for efficient forward SRS generation is above 4 μJ ($\sim$30 P_{cr}), which means that a dense plasma environment is necessary for fs filamentation induced SRS generation in water.

With a single probe beam undergoing filamentation in pure water and the long-pass filter to filter out the 400 nm signal, we measured the Raman intensity at 463 nm and its dependence upon the fs pump pulse energy, as shown in Figs. 3(a) and 3(b). For a limited detection capability of the power meter, Raman intensity was characterized by measuring the spectral intensity at 463 nm when input pulse energy of the probe beam was below 20 μJ, during which 10 laser shots were accumulated to reduce errors. When input pulse energy was above 10 μJ, we directly measured the output Raman energy and calculated the conversion efficiency meanwhile, as shown in Fig. 3(b). Raman intensity experienced a slow growth when input pulse energy was low (<4 μJ), and SPM induced continuum background and the onset of SRS are responsible for it. When input pulse energy was above 4 μJ, Raman intensity increased steadily with the pump energy. The Raman conversion efficiency also increased with pump energy

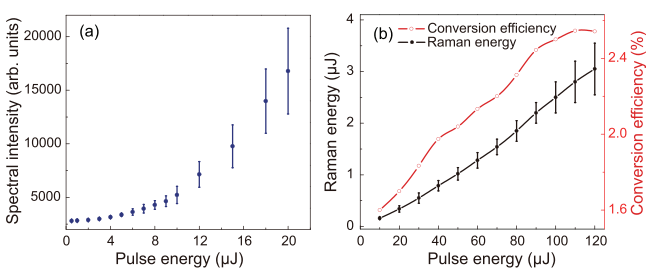

FIG. 3. Raman intensity of the probe beam as a function of the input pulse energy when a single beam underwent filamentation in water. (a) Raman intensity was characterized using the spectrometer when the input pulse energy was below 20 μJ. (b) Raman energy and Raman conversion efficiency were directly measured when the input pulse energy was above 10 μJ.

and approached saturation at 100 μJ to its maximum of about 2.5%. The tendency of the conversion efficiency as pump energy increased agreed with the experimental results observed with nanosecond lasers,[10,11] but the efficiency was much smaller. We attributed this to the temporal walk-off of the pump pulse and the Stokes Raman pulse as the ultrashort laser propagated in water due to normal GVD.

Let us consider a chirp-free 100-fs pulse with initially synchronous 400- and 463-nm components linearly propagating in water. After co-propagating L = 10 mm, the GVD will lead to a temporal walk-off of about $\Delta\tau = L \cdot \Delta n_g/c \approx 266 fs$ between the two spectral components with the 463-nm pulse propagating ahead, where n_g is the group index and the wavelength-related values are 1.363 and 1.355 for 400- and 463-nm components, respectively.[27] It means that only a very limited Raman gain length is available for fs Raman conversion in water, and it accounts for the high critical pulse energy for Raman emergence in our experiments, namely, only when plasma density reaches a certain value and extends for a moderate length will Raman conversion become efficient. Although the interplay of optical Kerr self-focusing, plasma defocusing, and pulse splitting due to the normal GVD during laser filamentation in water leads to abstruse pulse temporal and spatial reshaping,[6,24] the intuitive picture of this process can be understood as follows: When intense fs pulses propagate in water, the leading edge of the pulse ionizes water molecules mainly through multiphoton ionization (MPI) and generates plasma,[28] which will exert an influence on the following part of the pulse, during which plasma plays its role by creating an environment with refractive indexes below unit and anomalous dispersion. The group velocity of light travelling in plasma is expressed as $v_g = c\sqrt{1-\omega_p^2/\omega^2}$, where $\omega_p = \sqrt{n_e e^2/\varepsilon_0 m}$ is the plasma frequency of the free electron gas, n_e is the plasma density, e and m are the electric charge and effective mass of the electron, respectively, and ε_0 is the permittivity of free space.[29] It implies that in plasma the 400-nm pulse travels faster than the 463-nm pulse, and their group velocity difference increases with n_e, which is just the opposite of normal GVD in water and can make some compensation for it. For rough estimation, we take the typical value of the peak electron density as the laser undergoes filamentation in water of the order $10^{25} - 10^{26}/m^3$, which is obtained at 532 nm excitation.[28,30] After co-propagating L = 10 mm, a compensation of $8 - 80 fs$ will be made for the temporal walk-off of the 400-nm pulse and the 463-nm pulse. Considering the actual situation where the pulses propagate in a mixture of plasma and neutral water molecules, and furthermore, the plasma density created by UV filamentation and a relatively tight focusing in our case could be even greater,[6,21] the compensation of the walk-off by plasma is thus rather considerable. As the input pulse energy increased, the generated plasma channel became denser and the volume of the plasma channel expanded transversely,[17] which allowed Raman conversion in a larger transection. This was directly verified by the increasing output light spot of the Raman pulse as we increased the input pulse energy.

By following this idea, if we injected a pump beam into water and steered it to interfere with the probe beam to form

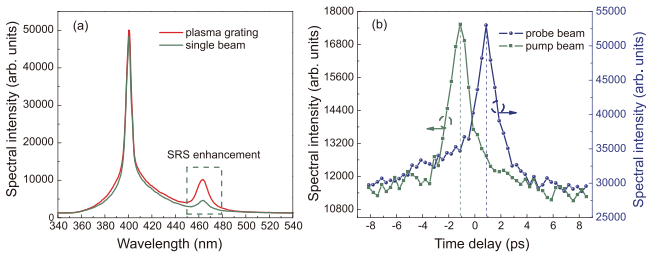

FIG. 4. (a) Raman enhancement of the probe beam by plasma grating when the time delay was 1 ps. (b) Raman intensities of the two beams as a function of the time delay. Positive values of the time delay denoted the pump beam travelling ahead of the probe beam. Note that the Raman spectral intensities of two beams cannot be compared crosswise, because the spectra collecting efficiency is different in two cases. The pulse energies of the probe beam and the pump beam were 50 and 35 μJ, respectively.

plasma grating in their intersection region, significant enhancement of Raman conversion of the probe beam should be observed due to the enhanced electron density of plasma grating.[17] Figure 4(a) presents the experimentally observed SRS enhancement of the probe beam when two beams form plasma grating in pure water. The pulse energies of the probe beam and the pump beam were 50 and 35 μJ, respectively, and the output Raman energy of the probe beam increased from 1.02 μJ to 1.67 μJ when the pump beam was turned on. As the two beams were almost the same and their Raman conversion benefited from the interacting plasma grating, we measured the Raman intensities of both beams versus the time delay, as shown in Fig. 4(b). Positive values of the time delay are referred to the pump beam travelling ahead of the probe beam. The Raman intensities were characterized by their spectral intensity at 463 nm, which were averaged over 10 sequential shots, and the error bars were omitted with the displayed data being their expectancy values. The Raman signal of both beams got enhanced in a temporal range with a FWHM of ~2 ps, which was much larger than the input pulse duration while within the lifetime of plasma in water.[31] There is no doubt that the pulses were temporally broadened due to dispersion when propagating in water. Raman enhancement existed during the whole life of plasma grating as we steered the time delay. From the point of view of pulse evolution, the overlapping part of two pulses generated ultradense plasma due to interference, which could act as a buffer area for pulse self-compression, and it further compensated the GVD of the pump pulse and the Stokes pulse, as schematically shown in Fig. 1. Interestingly, the maximum of the Raman intensities for both beams was not at the zero time delay point but at a delay of ~1 ps with the other beam propagating ahead. Note that for UV fs filamentation, the effect of electron impact ionization due to inverse bremsstrahlung is rather small,[6] so the avalanche ionization model should not be responsible for it. On the other hand, it can be easily understood as we consider the chirp and temporal broadening of the pulse. Here, we take the probe beam as the analysis case. As analyzed above, the Raman component mainly occupies the front edge of the pulse due to the dominant GVD, and the duration of the whole pulse is extended to the order of picosecond. So, when the front edge (Raman component) of the probe pulse synchronizes with the main part (400-nm component) of the pump pulse, the compensation reaches its best condition and finally results in the highest Raman conversion efficiency. While when the probe pulse travels in advance of the pump pulse, in which the main part (400-nm component) of the probe beam overlaps the front edge (Raman component) of the pump pulse, the SRS enhancement still exists but is not so significant. It is because this kind of overlapping can also result in local higher electron density, and the Raman conversion of the remaining part of the probe pulse still benefits from it.

In summary, we have experimentally observed intense forward SRS emission in water with fs UV filamentation at 400 nm. The results supplemented fs filamentation research at UV wavelength in water with significant SRS emission. Plasma density was shown to play an important role for efficient Raman conversion in compensating the normal GVD of pump pulse and Stokes Raman pulse in water, and this was verified by the enhancement of Raman conversion at plasma grating cases. Although the theoretical explanation to this phenomenon is rather rough in this paper, it provides a clear physical picture for the fs filamentation induced SRS process in water. The details of fs UV pulses propagating in water remain carefully explored. Our work may enlighten efficient Raman laser generation and fs Raman applications.

This work was supported by the National Key Scientific Instrument Project (2012YQ150092), National Natural Science Fund of China (11434005, 11621404, and 11727812), and Shanghai Education Commission (2017-01-07-00-05-E00021).

[1]J. Kasparian, M. Rodriguez, G. Mejean, J. Yu, E. Salmon, H. Wille, R. Bourayou, S. Frey, Y. B. André, A. Mysyrowicz, R. Sauerbrey, J. P. Wolf, and L. Wöste, Science **301**, 61 (2003).
[2]M. Rodriguez, R. Sauerbrey, H. Wille, L. Wöste, T. Fujii, Y. B. André, A. Mysyrowicz, L. Klingbeil, K. Rethmeier, W. Kalkner, J. Kasparian, E. Salmon, J. Yu, and J. P. Wolf, Opt. Lett. **27**, 772 (2002).
[3]D. Wang, W. Li, L. Ding, and H. Zeng, Opt. Lett. **39**, 4140 (2014).
[4]F. Théberge, N. Aközbek, W. Liu, A. Becker, and S. L. Chin, Phys. Rev. Lett. **97**, 023904 (2006).
[5]D. Faccio, A. Averchi, A. Dubietis, P. Polesana, A. Piskarskas, P. Di Trapani, and A. Couairon, Opt. Lett. **32**, 184 (2007).
[6]A. Couairona and A. Mysyrowicz, Phys. Rep. **441**, 47 (2007).
[7]D. Faccio, A. Averchi, A. Couairon, M. Kolesik, J. V. Moloney, A. Dubietis, G. Tamošauskas, P. Polesana, A. Piskarskas, and P. Di Trapani, Opt. Express **15**, 13077 (2007).
[8]M. Kolesik, E. M. Wright, and J. V. Moloney, Phys. Rev. Lett. **92**, 253901 (2004).
[9]D. Faccio, M. A. Porras, A. Dubietis, F. Bragheri, A. Couairon, and P. Di Trapani, Phys. Rev. Lett. **96**, 193901 (2006).
[10]M. H. Helle, T. G. Jones, J. R. Peñano, D. Kaganovich, and A. Ting, Appl. Phys. Lett. **103**, 121101 (2013).
[11]Y. Ganot, S. Shrenkel, B. D. Barmashenko, and I. Bar, Appl. Phys. Lett. **105**, 061107 (2014).
[12]Z. Li, X. Shan, Z. Li, J. Cao, M. Zhou, Y. Wang, Z. Men, and C. Sun, Appl. Phys. Lett. **101**, 021908 (2012).
[13]B. Hafizi, J. P. Palastro, J. R. Peñano, D. F. Gordon, T. G. Jones, M. H. Helle, and D. Kaganovich, Opt. Lett. **40**, 1556 (2015).
[14]V. R. Kumar and P. P. Kiran, Opt. Lett. **40**, 2802 (2015).
[15]H. Yui and T. Sawada, Phys. Rev. Lett. **85**, 3512 (2000).
[16]M. Sceats, S. A. Rice, and J. E. Butler, J. Chem. Phys. **63**, 5390 (1975).
[17]F. Liu, S. Yuan, B. He, J. Nan, M. Jiang, A. Q. Khan, L. Ding, J. Yu, and H. Zeng, Opt. Express **25**, 22303 (2017).
[18]Y. Liu, M. Durand, S. Chen, A. Houard, B. Prade, B. Forestier, and A. Mysyrowicz, Phys. Rev. Lett. **105**, 055003 (2010).
[19]Y. Zhao, T. E. Witt, and R. J. Gordon, Phys. Rev. Lett. **103**, 173903 (2009).
[20]R. Kupfer, B. Barmashenko, and I. Bar, Phys. Rev. E **88**, 013307 (2011).

[21]L. Shi, W. Li, Y. Wang, X. Lu, L. Ding, and H. Zeng, Phys. Rev. Lett. **107**, 095004 (2011).
[22]S. Suntsov, D. Abdollahpour, D. G. Papazoglou, and S. Tzortzakis, Appl. Phys. Lett. **94**, 251104 (2009).
[23]Y. Liu, M. Durand, A. Houard, B. Forestier, A. Couairon, and A. Mysyrowicz, Opt. Commun. **284**, 4706 (2011).
[24]A. Jarnac, G. Tamosauskas, D. Majus, A. Houard, A. Mysyrowicz, A. Couairon, and A. Dubietis, Phys. Rev. A **89**, 033809 (2014).
[25]S. Tzortzakis, B. Lamouroux, A. Chiron, S. D. Moustaizis, D. Anglos, M. Franco, B. Prade, and A. Mysyrowicz, Opt. Commun. **197**, 131 (2001).
[26]J. Schwarz, P. Rambo, J. C. Diels, M. Kolesik, E. M. Wright, and J. V. Moloney, Opt. Commun. **180**, 383 (2000).
[27]G. M. Hale and M. R. Querry, Appl. Opt. **12**, 555 (1973).
[28]A. Dubietis, A. Couairon, E. Kučinskas, G. Tamošauskas, E. Gaižauskas, D. Faccio, and P. Di Trapani, Appl. Phys. B **84**, 439 (2006).
[29]S. A. Maier, *Plasmonics: Fundamentals and Applications* (Springer, 2007).
[30]N. Tsuda, T. Yamaguchi, and J. Yamada, J. Plasma Fusion Res. Ser. **8**, 619 (2009), available at https://www.researchgate.net/publication/242775026_Property_of_Laser-Induced_Plasma_in_Liquid.
[31]C. B. Schaffer, N. Nishimura, E. N. Glezer, A. M.-T. Kim, and E. Mazur, Opt. Express **10**, 196 (2002).